Journal of Alloys and Compounds 509 (2011) 9255–9263

Contents lists available at ScienceDirect

Journal of Alloys and Compounds

journal homepage: www.elsevier.com/locate/jallcom

Controlled morphologies and optical properties of ZnO films and their photocatalytic activities

Jingjing Duan, Xiaoheng Liu*, Qiaofeng Han, Xin Wang*

Key Laboratory for Soft Chemistry and Functional Materials, Nanjing University of Science and Technology, Ministry of Education, Nanjing 210094, China

ARTICLE INFO

Article history:
Received 9 April 2011
Received in revised form 8 July 2011
Accepted 8 July 2011
Available online 18 July 2011

Keywords:
Oxide materials
Thin films
Crystal growth
Crystal structure
Optical spectroscopy

ABSTRACT

ZnO films with three different microstructures including hexagonal prisms, plates and rose-like twinned crystals were fabricated using chemical bath deposition with different concentration of gelatin. The growth mechanisms of ZnO films were discussed, and the gelatin played a vital role as a polyelectrolyte capping the formation of microstructures. The photoluminescence and Raman properties were found sensitive to the crystal morphologies of ZnO films. Significantly, the photodegradation efficiencies of methylene blue under UV light irradiation in the presence of ZnO films consisted of hexagonal prisms and rose-like twinned crystals were 95% and 96%, respectively. The excellent photocatalytic activities can be ascribed to the high oxygen vacancies concentration and high percentage of polar planes, and this result was important in addressing the origin of high photocatalytic activity.

1. Introduction

Zinc oxide (ZnO), with a wide band gap of 3.37 eV and a large exciton binding energy of 60 meV, is one of the most versatile semiconductor materials and exhibits a myriad of nano/micromorphologies, such as rods, tubes, slices, doughnuts, nanocorals, hourglass-like, chestnut-like and flower-like shapes [1–8]. Recently, ZnO and especially doped ZnO are investigated in a wide range of applications such as ultraviolet emitting, thin film transistors, solar cells, and photocatalysis [9–13].

Generally, the growth of ZnO nano/microstructures is realized through three methods: vapor phase process, melt growth, and solution phase synthesis [14–16]. In comparison with vapor phase and melt methods, solution phase method is remarkable for their cheap experimental setups, large productivity, and mild conditions. Chemical bath deposition (CBD) is one of the useful solution methods for film deposition from aqueous solution containing precursors, complexing agents, and pH buffers [17,18]. Its advantages include not only low processing temperature, not requiring vacuum systems, allowing growth upon a variety of substrates, but also its compatibility with large area deposition, which is low cost, energy saving, industrial-scale and environmentally benign.

Recent years, the morphology-controlled synthesis of metallic oxides has received much attention to produce highly functional materials, because of their special morphology-structure-function relationship. Younan Xia et al. have reported the shape control of noble-metal nanocrystals including Ag, Pt, Au, Pd, and Rh [19–23]. Xie and co-workers have demonstrated the morphological control synthesis of Co_3O_4 nanorod clusters, preferentially exposing the plane rich in Co^{3+} sites which exhibit high catalytic activity for CO oxidation [24]. Yang et al. have synthesized uniform anatase TiO_2 single crystals with high percentages of [0 0 1] facets (47% and 64%) using hydrofluoric acid and 2-propanol as the morphology controlling agent, which is promising in solar cells, optoelectronic devices and photocatalysis [25,26].

Herein, we report the morphology-controlled synthesis of ZnO films with gelatin via CBD. Different ZnO microstructures ranging from hexagonal prisms, plates to rose-like twinned crystals are prepared through varying the concentration of gelatin. Further, the growth mechanisms of ZnO microstructures have been discussed. Above all, the ZnO films consisted of hexagonal-prisms and rose-like twinned crystals exhibit excellent photocatalytic activities with less catalyst quantity and high efficiency, compared with reported ZnO and doped ZnO powders and films [12,13,27–29].

2. Experimental details

2.1. Materials

Zinc acetate dihydrate (≥99.0% purity, Sinopharm Chemical Reagent Co., Ltd, China), gelatin (type A, for analysis, granular, Acrös Organics, molecular weight 100,000 g/mol), and methylene blue (MB, ≥98.0% purity, Sinopharm Chemical Reagent Co., Ltd, China) were used without further purification. Microscope slides (Sail Brand Cat. No. 7101) were used as the supporting substrates, which were cleaned ultrasonically in distilled water and ethanol for 15 min, respectively.

* Corresponding authors. Tel.: +86 25 8431 5943; fax: +86 25 8431 5054.
E-mail addresses: xhliu@mail.njust.edu.cn, duanjingjingcopy@163.com (X. Liu), wangx@mail.njust.edu.cn (X. Wang).

0925-8388/$ – see front matter © 2011 Elsevier B.V. All rights reserved.
doi:10.1016/j.jallcom.2011.07.017

2.2. Synthesis

In a typical procedure, a 60 mL of 0.2 M zinc acetate aqueous solution was prepared at room temperature. Gelatin was dissolved in 60 mL of distilled water at about 40 °C and added to zinc acetate solution stirred. Then the glass substrate was immersed into the mixture. This was sealed and left undisturbed at 95 °C. After several hours, the glass substrate was washed several times with deionized water and dried in air at ambient condition. For the transmission electron microscopy (TEM) and thermogravimetric analysis (TG) measurements, the powder sample was peeled from the substrate. For other measurements, the as-prepared sample on the substrate was used.

2.3. Characterization

The crystal phase and purity of the products were determined with powder X-ray diffraction (XRD, Bruker D8 Advance diffractometer using Cu Kα radiation, λ = 1.5418 Å). The structural and morphological analyses of the samples were obtained with scanning electron microscopy (SEM, JEOL-6380LV), field-emission scanning electron microscopy (FESEM, LEO-1550) equipped with an energy dispersive X-ray spectrometer (EDS) unit, and TEM (JEOL-2100). Photoluminescence (PL) measurements were conducted with a FL3-TCSPC fluorescence spectrometer, excited by a 327 nm He-Cd laser. Raman spectra were recorded on a Renishaw Micro-Raman spectrometer, with an excitation line at 514.5 nm provided by an argon ion

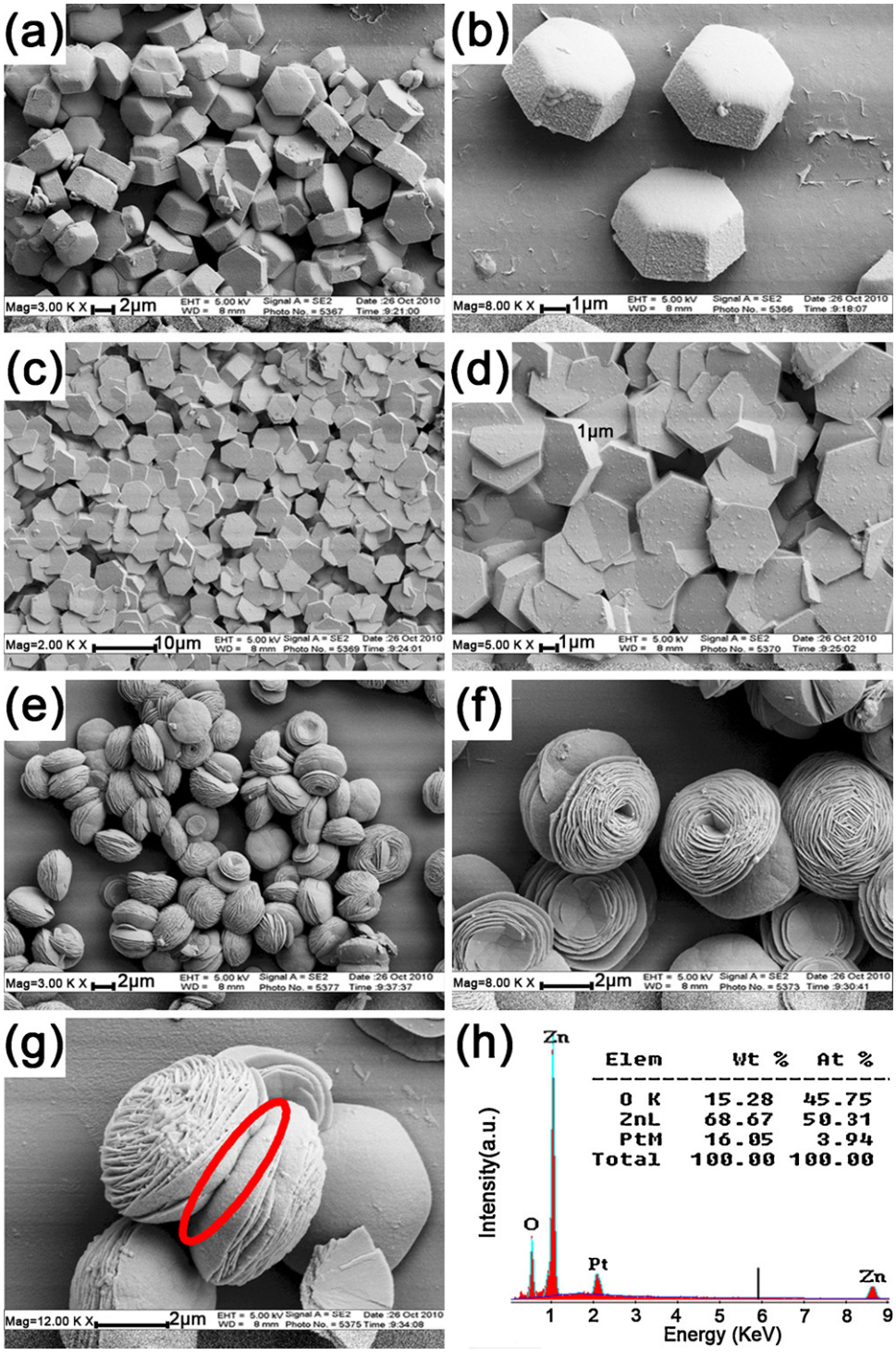

Fig. 1. FESEM images of ZnO films obtained with gelatin (a, b) 0 μM; (c, d) 10 μM; (e–g) 125 μM for 6 h; (h) EDS analysis of rose-like ZnO twinned crystals.

laser. The transmittance and diffuse reflection spectroscopy (DRS) measurements were carried out on a Shimadzu UV-2550 spectrophotometer equipped with an integrated sphere. $BaSO_4$ was used as a reference. TG of ZnO powers was performed on a TGA/SDTA851e thermogravimetric analyzer from 50 to 900 °C at a heating rate of 10 °C/min, with N_2 flow of 30.0 mL/min.

2.4. Photocatalysis

The photocatalytic activities of as-synthesized ZnO films were evaluated by the photodecomposition of MB under UV irradiation with 500 W high-pressure Hg lamp at room temperature (RT). The detailed experimental procedure can be described as follows: a piece of ca. 2.5 cm × 2.5 cm as-prepared ZnO film was immersed in 400 mL of 20 mg/L MB aqueous solution with a magnetic stirrer bar and bubbling air at a flow rate of 0.1 L/min. The efficiency of the degradation process was monitored though the absorption at the maximum absorption around λ_{max} = 664 nm as a function of irradiation time, using a BRAIC UV-1201 spectrophotometer.

3. Results and discussion

3.1. Morphology-controlled synthesis of ZnO films

Fig. 1 shows the FESEM images of the as-synthesized ZnO films with different morphologies. As illustrated in Fig. 1a and b, unoriented ZnO hexagonal prisms with a height and a rim both of 1 μm, are observed in the absence of gelatin. While in the presence of a small quantity of gelatin (10 μM), densely packed hexagonal ZnO plates with a rim of 3 μm are obtained (Fig. 1c, d). As the gelatin is further increased to 125 μM (Fig. 1e–g), only rose-like ZnO crystals are acquired, consisting of self-assembled slices which are tens of nanometers in thickness and several micrometers in diameter. In addition, from the side view of rose-like ZnO, we can see that ZnO crystals are twinned (circled area in Fig. 1g). A typical EDS spectrum of rose-like ZnO twinned crystals shows that only O and Zn elements are the main components (Fig. 1h), besides the platinum signal from the sample preparation for the EDX measurement.

To understand the interactions between the films and the substrates, the cross-section of ZnO films are illustrated in Fig. S1. We can see that the films are grown from the substrates but not continuous. Furthermore, the adhesion between the particles and the substrates has been tested with the Scotch tape test, which is commonly used to measure the adhesion strength of thin films to substrates [30]. In the test, we repeatedly applied adhesive tape to the film and then pulled it off, up to 30 times. The morphology and UV–vis transmittance before and after the Scotch tape test have been characterized, as shown in Figs. S2 and S3. For the ZnO film prepared without gelatin, unoriented hexagonal prisms have been peeled off extensively from the substrate and considerable residual impurities from the Scotch tape are observed. As expected, the transmittance at 368 nm (the absorption threshold, UV region) of the film has changed noticeably, from 67% of the initial film to 78% of its counterpart after peeled off for 30 times with Scotch tape. Noteworthily, the morphology and transmittance only subject to insignificant changes for the ZnO films prepared with gelatin. The packed hexagonal plates and rose-like ZnO films show both superior mechanical strength and stability to the unoriented ones. It is suspected that gelatin, a conventional polymer, may also interact with the glass substrate apart from serving as templates in crystal growth process, giving durable functional films.

Fig. 2 shows the XRD patterns of the as-synthesized ZnO films, which can be attributed to the wurtzite hexagonal ZnO (JCPDS 36-1451) with the lattice constants *a* and *c* of 0.325 nm and 0.521 nm, respectively. However, the relative intensities of the corresponding XRD peaks are not exactly matched the standard XRD pattern of ZnO (JCPDS 36-1451). The (0 0 0 2) reflection is so strong that other reflections are nearly invisible or neglectable. The strong (0 0 0 2) peak reflects the structures of as-synthesized samples are [0 0 0 1]-oriented or with large surface area of polar (0 0 0 1) and (0 0 0 $\bar{1}$) facets [3]. The hexagonal prisms in the ZnO film prepared without gelatin are [0 0 0 1]-oriented and sufficiently thick for the relative

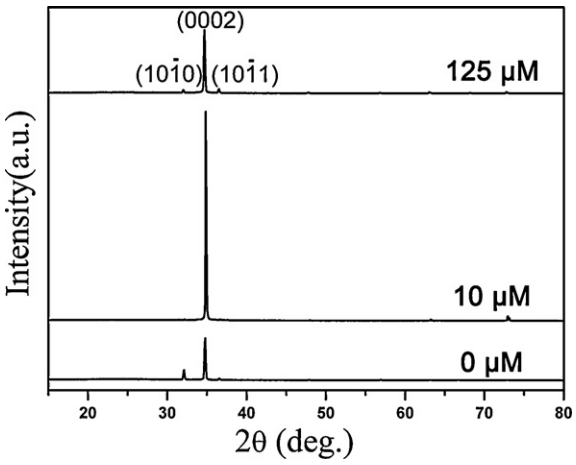

Fig. 2. XRD patterns of ZnO films obtained with gelatin: 0, 10 and 125 μM for 6 h.

intensities to reflect this orientation. The densely packed hexagonal ZnO plates are extremely well [0 0 0 1]-oriented and with greatly large surface area of polar facets. And the rose-like film consisted with ZnO slices are with extremely large surface area of polar facets.

The products have also been investigated by TEM and HRTEM, as shown in Fig. 3. Fig. 3a shows the TEM image of the hexagonal prisms ZnO film prepared without gelatin; hexagons and some fragments are observed. HRTEM image in Fig. 3b displays the lattice fringe with a spacing of 0.283 nm corresponding to the (0 1 $\bar{1}$ 0) plane of ZnO, indicating high crystallinity of the as-prepared ZnO film. Its Fast Fourier Transform (FFT) image has revealed the characteristics of a single crystal, as seen in the inset of Fig. 3a. Fig. 3c and d displays the TEM and HRTEM images of the hexagonal ZnO plates prepared with 10 μM gelatin, giving regular hexagons with a rim of about 3 μm, which is in agreement with the FESEM results. TEM image of the rose-like ZnO twinned crystals obtained from 125 μM gelatin is shown in Fig. 3e. The ZnO crystals are circular; and fragments of rose-like products are observed. In addition, HRTEM image of rose-like ZnO products is shown in Fig. 3f.

3.2. Growth process of rose-like ZnO twinned crystals

In order to investigate the growth process of rose-like ZnO twinned crystals, we carried out time dependent experiments (Fig. 4). At a growth time of 0.5 h, there are small quantities of rose-like ZnO like a few dispersive islands, as shown in Fig. 4a. Then at a growth time of 2 h, the twinned crystals grow into clusters, as seen in Fig. 4b. When the growth time is increased to 4 h, well-aggregated islands are obtained, as shown in Fig. 4c. A larger scale twinned crystals of ZnO are seen for a growth time of 6 h (Fig. 4d).

Fig. 5 shows the XRD patterns of rose-like the ZnO films prepared with 125 μM gelatin for various growth durations. All of the ZnO samples show a similar XRD pattern having the predominant (0 0 0 2) plane. Noticeably, the intensity of (0 0 0 2) peaks increase proportionally with time, showing that the amount of ZnO twinned crystals increases with time. This is in agreement with SEM observation shown in Fig. 4.

3.3. Growth mechanism of ZnO films

The following chemical reactions take place in the aqueous solution, resulting in formation of the ZnO:

$$CH_3COO^- + H_2O \rightarrow CH_3COOH + OH^- \quad (1)$$

$$Zn^{2+} + 4OH^- \rightarrow Zn(OH)_4{}^{2-} \quad (2)$$

$$Zn(OH)_4{}^{2-} \rightarrow ZnO \quad (3)$$

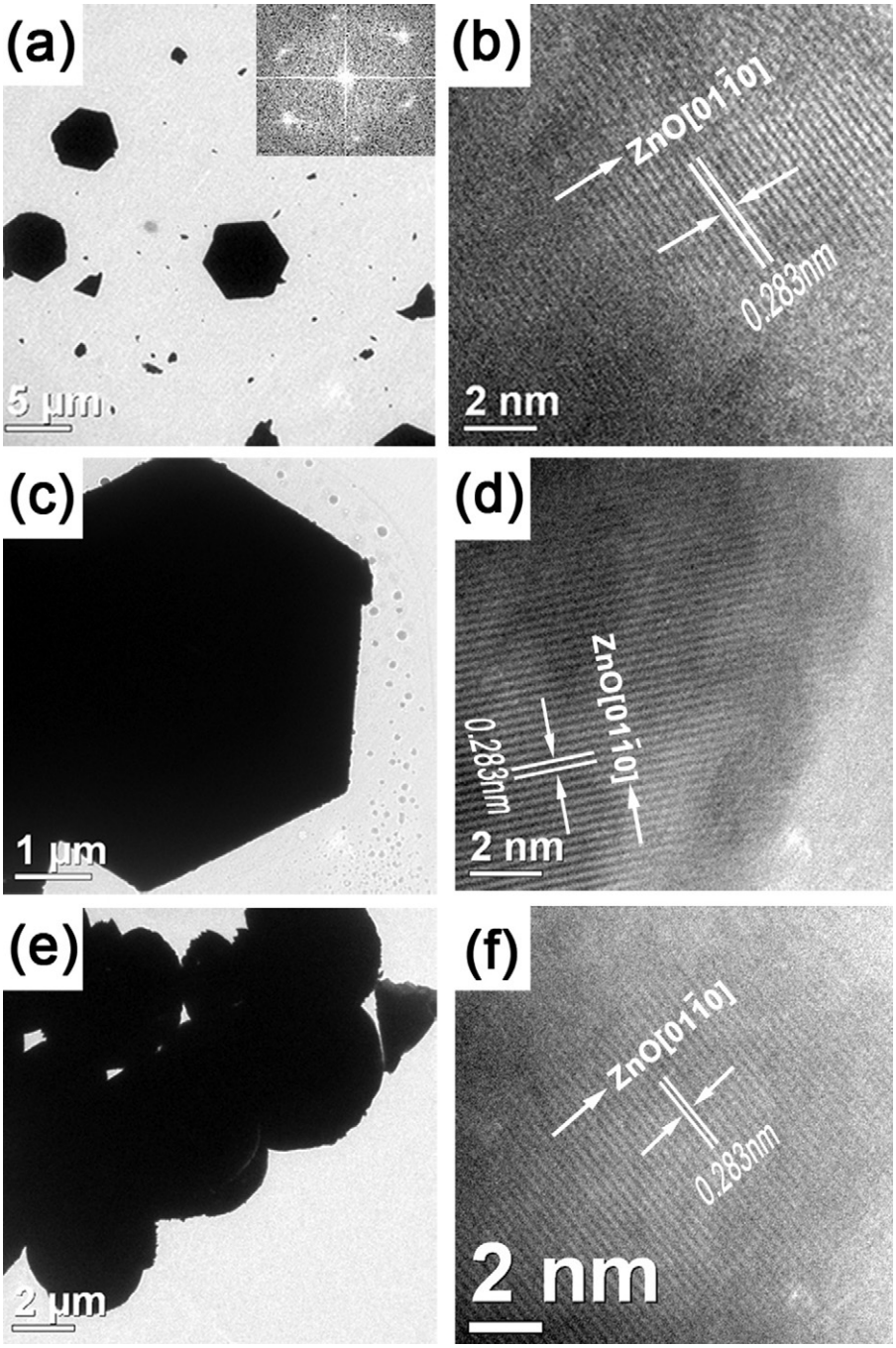

Fig. 3. TEM and HRTEM images of ZnO films obtained with gelatin (a, b) 0 μM; (c, d) 10 μM; (e, f) 125 μM.

The growth procedure of crystals usually contains the formation of growth unit and incorporates this at the interface [31,32]. The growth unit of the ZnO crystal is the coordination polyhedron $Zn(OH)_4^{2-}$, as shown in Scheme 1a, which is connected with each other sharing O^{2-} in the interior of the crystal. The growth habit of ZnO crystal is due to the different growth rates at various crystal faces, which is found as followed: $V_{[0001]} > V_{[01\bar{1}1]} > V_{[01\bar{1}0]} > V_{[000\bar{1}]}$, shown in Scheme 1b.

In Scheme 2, the growth mechanisms of ZnO films with different microstructures are discussed. A large number of ZnO nanocrystallines are first formed due to supersaturation of the precursor solution. In the absence of gelatin during the preparation (step I in Scheme 2), the growth unit $Zn(OH)_4^{2-}$ grows along its growth habit [0 0 0 1] direction. Nevertheless, the OH^- ligands at the interface of the crystal prevent the new $Zn(OH)_4^{2-}$ ions from incorporating effectively into the as-formed ZnO nanocrystallines along the [0 0 0 1] direction [31]. This means that the crystal growth along the [0 0 0 1] direction is partially suppressed, hence only hexagonal prisms (Scheme 2a) are synthesized rather than 1D ZnO structures (Scheme 1b).

The isoelectric point (IEP) of A-gelatin in water is around 8. The pH values of 0.2 M $Zn(AC)_2$ solution, 10 μM and 125 μM gelatin solution are measured to be 6.28, 5.49 and 5.28, respectively. And the pH values of mixed precursor solution ($Zn(AC)_2$ solution mixed with 10 μM and 125 μM gelatin) are 6.34 and 6.36, which are below the IEP of type-A gelatin, so gelatin is positively charged in the reaction solution. In the presence of 10 μM and 125 μM gelatin (step I in Scheme 2), the positive gelatin anchors on the O^{2-}-terminated

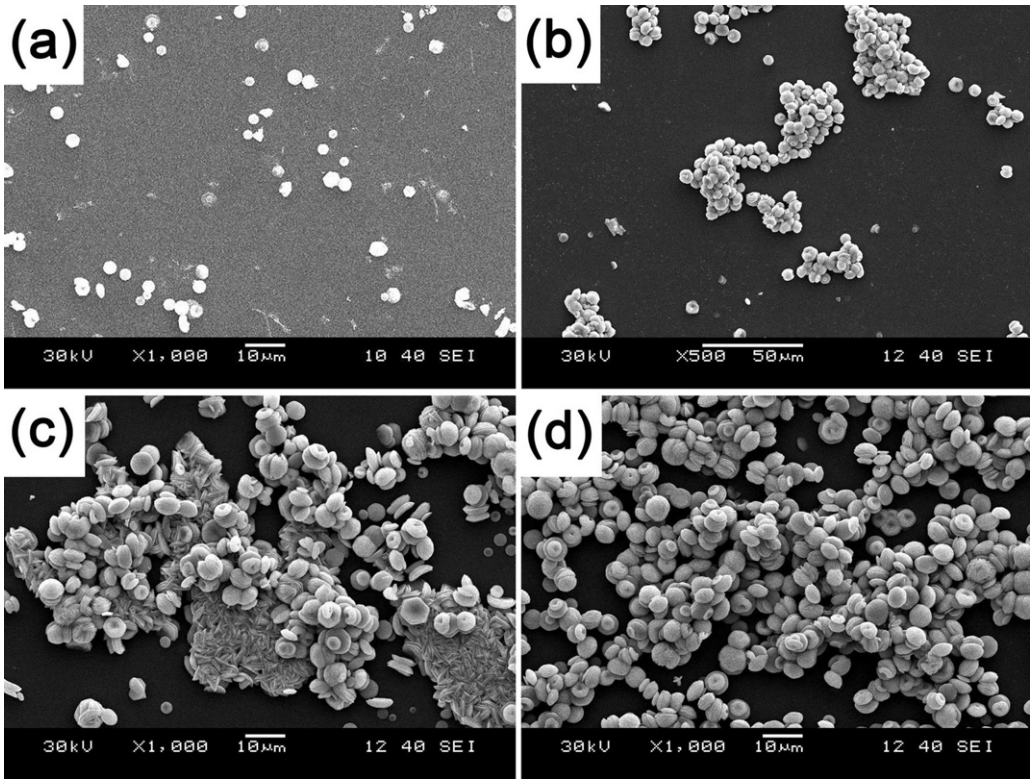

Fig. 4. SEM images of ZnO films obtained with 125 μM gelatin for various growth durations: (a) 0.5 h; (b) 2 h; (c) 4 h; (d) 6 h.

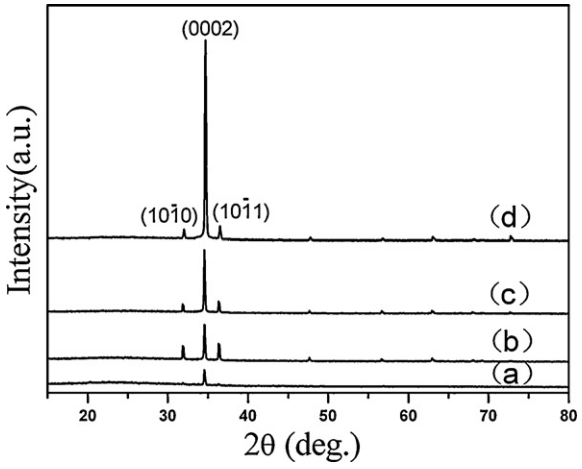

Fig. 5. XRD patterns of ZnO films with 125 μM gelatin for various growth durations: (a) 0.5 h; (b) 2 h; (c) 4 h; (d) 6 h.

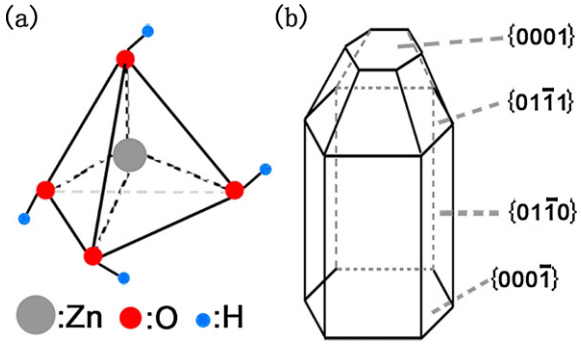

Scheme 1. (a) The growth unit of ZnO. (b) The growth habit of ZnO.

(0 0 0 $\bar{1}$) plane of ZnO nanocrystallines (Scheme 2b). Thus the crystal growth along [0 0 0 1] direction is suppressed due to electrostatic interactions. Adsorption of gelatin on the polar planes of ZnO changes the intrinsic anisotropy in the growth rates and makes ZnO nanocrystallines to grow sideways along [0 1 $\bar{1}$ 0] direction through oriented attachment [33] of the adjacent nanocrystallines. This results in the formation of 2D hexagonal ZnO plates (Scheme 2c).

In the presence of 125 μM gelatin (step III in Scheme 2), because of the strong electrostatic interactions between sufficient gelatin and ZnO nanocrystallines (Scheme 2d), lots of ZnO slices (Scheme 2e) appear in the beginning [34,35]. It has been reported that slight bending in ZnO plates result in grain boundaries to accommodate local strain (Scheme 2f) [36]. As the Zn^{2+}-terminated and O^{2-}-terminated planes align alternatively along [0 0 0 1] direction in the crystals, the structure of ZnO possesses an intrinsic dipole moment along [0 0 0 1] direction [37,38]. In order to counterbalance the dipolar field, two ZnO slices with opposite polar directions assemble together for charge neutralization and plane stabilization, resulting in the formation of ZnO twinned crystals [34,38,39]. The twinned phenomenon with the (0 0 0 1) or (0 0 0 $\bar{1}$) plane as the juncture occurs commonly in ZnO [5,35,40–42]. Although the dipole field in a twin crystal is mostly weakened, the surface nearby the brim of the ZnO twinned crystals still suffer a dipole field from the neighboring stacked slices. This results in the alignment of ZnO nanocrystallines in slices ranges in three dimensions along the dipole field (Scheme 2g) [34]. Eventually, the bowl-like networks are formed and serve as a substrate for newly growing ZnO slices. The twinned ZnO slices grow and assemble simultaneously on both sides due to charge interactions between the (0 0 0 1) plane of one ZnO slice and the (0 0 0 $\bar{1}$) plane of another one. Thus, the rose-like ZnO twinned crystals are obtained (Scheme 2h). In addition, the hexagonal faceted structure of ZnO slice transforms to a more circled shape to minimize total energy [43].

The gelatin contents in ZnO films are determined by TG, as shown in Fig. S4. The weight loss of hexagonal plates and rose-like

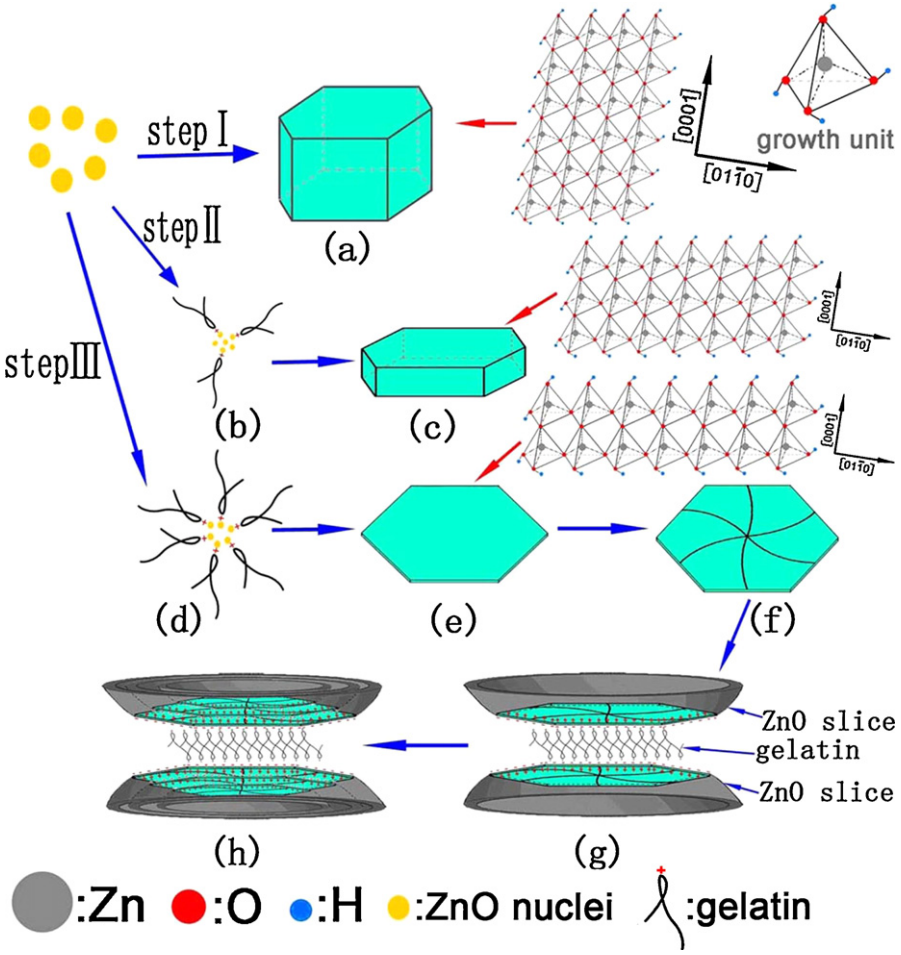

Scheme 2. The growth mechanism of ZnO films with different microstructures.

ZnO films between 209 °C and 900 °C is 11.8% and 6.2%, respectively. This is ascribed to the decomposition of gelatin, revealing a strong binding of gelatin on ZnO films. And the weight loss before 209 °C can be attributed to the water removal of ZnO films.

Furthermore, the amount effects of gelatin on the final formation of these structures have been further explored using SEM, as shown in Fig. S5. The concentrations of gelatin are varied from 1.7, 41.7, and 83.3 to 250 μM.

3.4. Optical properties

The photoluminescence spectrum is an effective method to evaluate both crystal defects and its optical properties. PL spectra of the ZnO crystals are shown in Fig. 6. Typically, the hexagonal prisms ZnO film obtained in the absence of gelatin, exhibits a strong and wide visible green emission around 568 nm. However, the hexagonal plates ZnO film prepared with 10 μM gelatin displays an UV emission around 390 nm with a full width at half-maximum (fwhm) of 47 nm and a neglectable green emission. The rose-like ZnO film prepared with 125 μM gelatin shows a strong UV emission around 394 nm with an fwhm of 60 nm.

The UV emission is generally attributed to the recombination of free excitons between conductive band and valence band, which is called near-band-edge emission [44–47]. For the green emission, it is usually believed that visible emissions are due to transition in defect states, particularly the oxygen vacancies [45,46,48]. The intense and sharp UV band edge emission of rose-like twinned crystals ZnO film indicates a high crystalline perfection. The shift in the UV peaks of the ZnO films prepared with gelatin can be ascribed to the difference in crystal sizes. However, the strong green emission around 568 nm of the hexagonal prisms ZnO film shows a high defect concentration such as oxygen vacancies in the product. The differences in the PL spectra of the samples synthesized under different conditions suggest that the optical properties of ZnO films are directly affected by the quality, sizes and structure defects of crys-

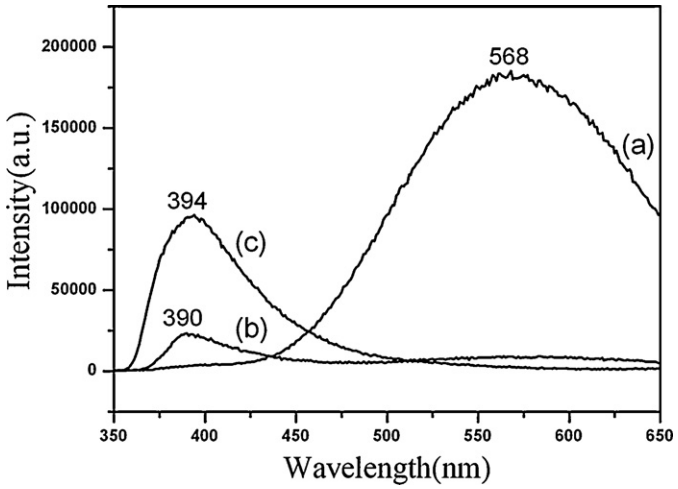

Fig. 6. RT photoluminescence spectra of ZnO films obtained with gelatin (a) 0 μM; (b) 10 μM; (c) 125 μM.

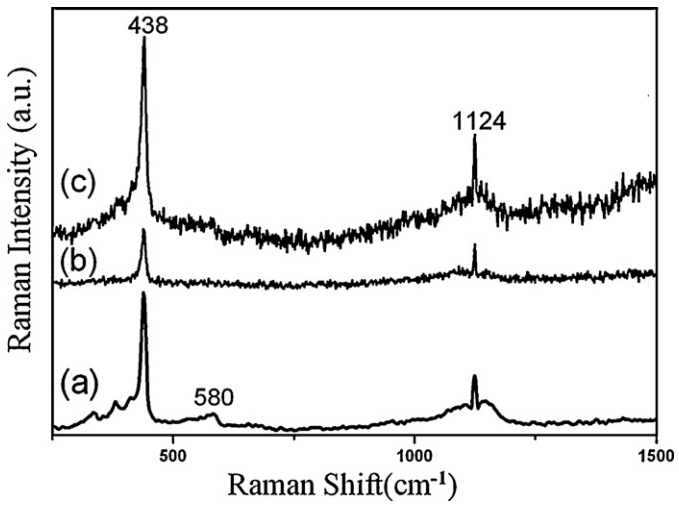

Fig. 7. The Raman spectra of ZnO films prepared with gelatin (a) 0 μM; (b) 10 μM; (c) 125 μM.

tals. Herein, different crystal morphologies have discrepant crystal qualities, sizes and structure defects. So we can conclude that the optical properties of ZnO films are sensitive to the crystal morphology of the film.

The Raman spectra of the as-prepared ZnO films are shown in Fig. 7. Wurtzite ZnO belongs to the space group $P6_3mc$, which has eight sets of phonon modes: $2E_2$, $2A_1$, $2E_1$ and $2B_1$, according to the group theory [49–51]. Among them, the $2B_1$ modes are neither Raman nor infrared active. Both A_1 and E_1 modes are polar and split into transverse optical (TO) and longitudinal optical (LO) phonons, all being Raman and infrared active. The two nonpolar E_2 modes are Raman active only. In Fig. 7, the lines around 438 cm^{-1} and 1123 cm^{-1} are assigned to ZnO E_2 and A_1 (LO) phonon mode, respectively. Generally the E_2 mode is ascribed to vibrations of tetrahedrally coordinated oxygen around zinc, representing the band characteristic of wurtzite phase. However, the appearance of the E_1 (LO) mode at 580 cm^{-1} in the hexagonal prisms ZnO film (Fig. 7a), is ascribed to oxygen deficiency [52,53], which confirms the PL investigation.

In addition, we have measured the DRS of these three ZnO films in order to obtain the band gap. As shown in Fig. S6, the spectra are given as plots of the Kubelka–Munk remission function (converted from the diffuse reflection values: $F(R) = (1-R)^2/2R$) vs energy (eV) [54–56]. The values of band-gap energy (Eg) are calculated to be 3.51 eV, 3.33 eV and 3.40 eV for ZnO films consisted of hexagonal prisms, densely packed hexagonal plates and rose-like twinned crystals, respectively. The difference between Eg values may be attributed to the microstructures, crystalline sizes, and defect levels of ZnO films. Further study is still in progress to address the variation of Eg.

3.5. Photocatalytic activities

Fig. 8 shows the absorption spectra and concentration changes as irradiation time of MB solution under UV photodegradation

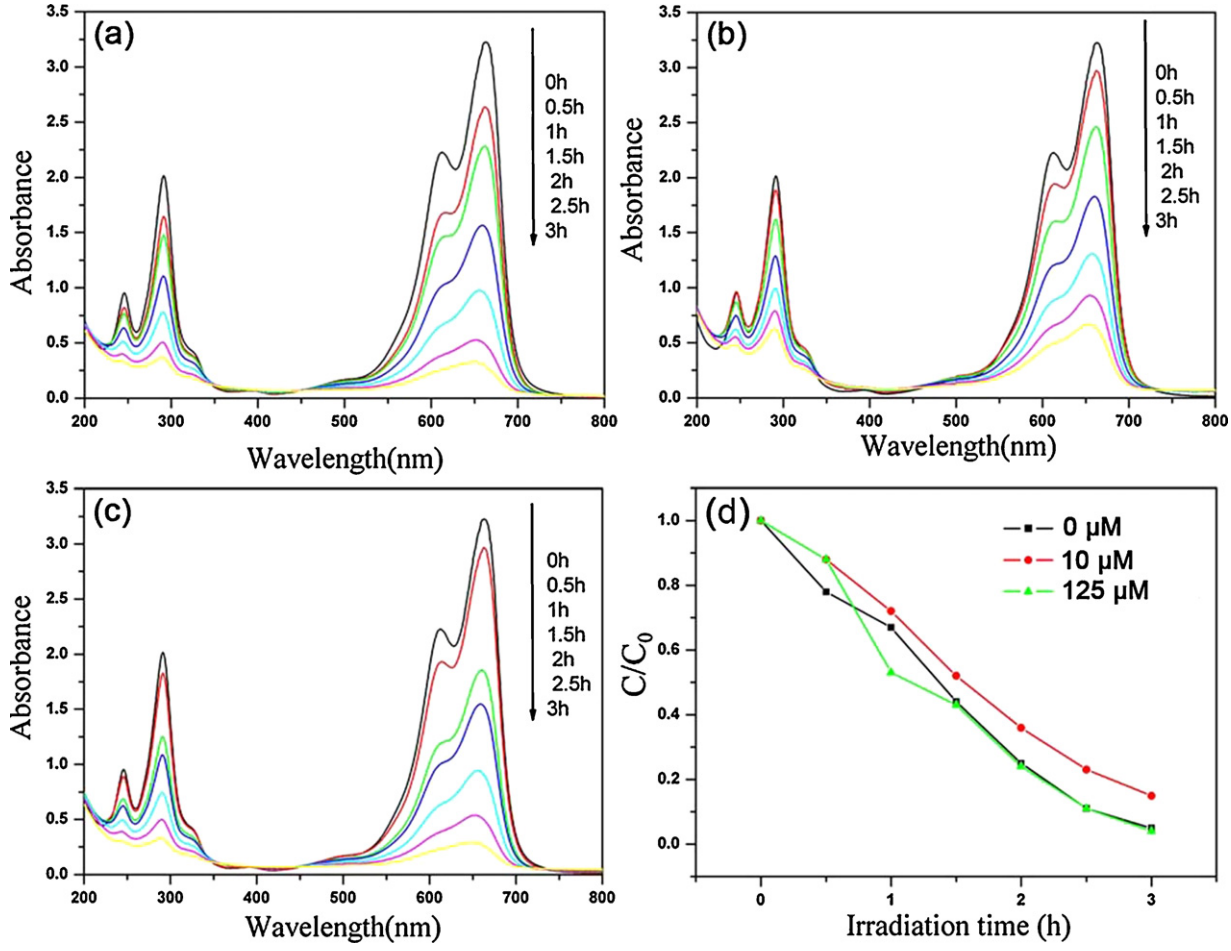

Fig. 8. Absorption spectra of MB solution under photodegradation with as-synthesized ZnO films using (a) 0 μM; (b) 10 μM; (c) 125 μM gelatin; (d) concentration changes of MB solution as a function of irradiation time.

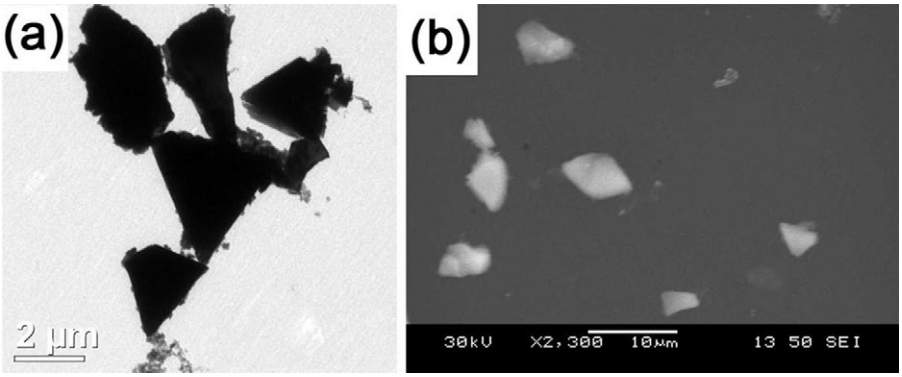

Fig. 9. Images of rose-like ZnO twinned crystals after the photocatalytic reaction: (a) TEM; (b) SEM.

with the as-synthesized ZnO films. The hexagonal prisms ZnO film exhibits exclusive photocatalytic activity; the efficiency is up to 95% at an irradiation time of 3 h. The ZnO film consisting of densely packed hexagonal plates, exhibits an efficiency of 84.5% at an irradiation time of 3 h. Furthermore, the rose-like ZnO film shows a standout photocatalytic activity with an efficiency of 96% after 3 h of irradiation.

In the photodegradation process of MB solution, the following reactions would occur:

$$ZnO + h\nu \rightarrow e_{cb}^{-} + h_{vb}^{+} \quad (4)$$

$$h_{vb}^{+} + OH^{-} \rightarrow OH^{\bullet} \quad (5)$$

$$h_{vb}^{+} + H_2O \rightarrow OH^{\bullet} + H^{+} \quad (6)$$

$$OH^{\bullet} + C_{16}H_{18}ClN_3S \rightarrow CO_2 \quad (7)$$

where $h\nu$ is the energy of a photon, e_{cb}^{-} is a electron in the conduction band, and h_{vb}^{-} is a hole in the valence band. The h_{vb}^{+} generated under the irradiation of UV light is a strong oxidizing agent and will react with H_2O and OH^{-} around ZnO, resulting in the formation of $OH^{\bullet}$ radicals. Also as a strong oxidizing agent, the $OH^{\bullet}$ radicals can react the organic compounds and decompose them to CO_2 [2,57]. The high efficiency of hexagonal prisms ZnO film can be attributed to high concentration of oxygen vacancies. It can be concluded that oxygen vacancies in ZnO would act as potential wells to trap electrons, aiding electron–hole pair separation and hence increasing the photocatalytic activity [12,58]. As for the twinned crystals ZnO film, the rose-like networks would disassemble into single slices during photocatalytic process, as observed by TEM and SEM (Fig. 9). This may be ascribed to that residual gelatin in ZnO film can be easily decomposed under UV irradiation with ZnO photocatalyst, destroying the durable film. Thus Zn^{2+}-terminated (0 0 0 1) plane of ZnO is exposed. The excellent photocatalytic activity of the twinned crystals ZnO film can be attributed to the high percentage of Zn^{2+}-terminated (0 0 0 1) face of ZnO, for that the OH^{-} ions in the dye solution would preferentially adsorb onto (0 0 0 1) face of ZnO because of its positive charge [12,57]. This would lead to a greater rate of production of $OH^{\bullet}$ radicals, promoting the degradation of dye. The unsatisfied photocatalytic activity of the hexagonal plates ZnO film can be ascribed to the low defect concentration and the decreased percentage of polar planes.

The calculated ZnO contents of the employed films consisting of hexagonal prisms, plates and rose-like twinned crystals in the dye solution is 7 mg/L, 17.7 mg/L and 13.7 mg/L, respectively. On the other hand, the catalyst quantities of ZnO powders are usually hundreds of milligrams per liter in the reported studies [12,27]. The photocatalytic activities of the ZnO films consisted of hexagonal prisms and rose-like twinned crystals obtained in this study towards MB have excellent potential as photocatalytic material, compared with previous reports [12,13,27–29].

4. Conclusions

ZnO films with three different morphologies have been controllably synthesized via CBD at 95 °C by changing the concentration of gelatin. FESEM, XRD, EDS, and TEM have been used to characterize morphologies and structures of as-prepared ZnO films; and hexagonal prisms, packed plates and rose-like twinned crystals are obtained. The growth mechanisms of ZnO films have been discussed. As a polyelectrolyte, gelatin acts as a capping reagent in the formation of ZnO hexagonal plates and rose-like twinned crystals. The photoluminescence and Raman properties are found related to the morphologies of ZnO films. The ZnO films consisting of hexagonal prisms and rose-like twinned crystals exhibit excellent photocatalytic efficiencies of 95% and 96% at 3 h, respectively, compared with reported results. The photocatalytic process using ZnO films displays several advantages in removing the residual catalysts and experimental process with comparison with powders.

Acknowledgments

We thank the Natural Science Foundation of China (No. 50772048) and the Natural Science Foundation of China and China Engineering Physics (No. 10776014). The authors thank Dr. Karthik Ramasamy, The Manchester Materials Science Centre and Department of Chemistry, University of Manchester, for his help with English revision.

Appendix A. Supplementary data

Supplementary data associated with this article can be found, in the online version, at doi:10.1016/j.jallcom.2011.07.017.

References

[1] D. Bekermann, A. Gasparotto, D. Barreca, L. Bovo, A. Devi, R.A. Fischer, O.I. Lebedev, C. Maccato, E. Tondello, G.V. Tendeloo, Cryst. Growth Des. 10 (2010) 2011–2018.
[2] D. Chu, Y. Masuda, T. Ohji, K. Kato, Langmuir 26 (2009) 2811–2815.
[3] X. Liu, M. Afzaal, K. Ramasamy, P. O'Brien, J. Akhtar, J. Am. Chem. Soc. 131 (2009) 15106–15107.
[4] T. Ghoshal, S. Kar, S. Chaudhuri, Cryst. Growth Des. 7 (2007) 136–141.
[5] K.X. Yao, R. Sinclair, H.C. Zeng, J. Phys. Chem. C 111 (2007) 2032–2039.
[6] S.L. Wang, X. Jia, P. Jiang, H. Fang, W.H. Tang, J. Alloys Compd. 502 (2010) 118–122.
[7] L. Feng, A. Liu, M. Liu, Y. Ma, J. Wei, B. Man, J. Alloys Compd. 492 (2010) 427–432.
[8] H.I. Abdulgafour, F.K. Yam, Z. Hassan, K. AL-Heuseen, M.J. Jawad, J. Alloys Compd. 509 (2011) 5627–5630.
[9] Q. Ma, T.E. Saraswati, A. Ogino, M. Nagatsu, Appl. Phys. Lett. 98 (2011) 051908.
[10] K. Song, J. Noh, T. Jun, Y. Jung, H.-Y. Kang, J. Moon, Adv. Mater. 22 (2010) 4308–4312.

[11] C. Xu, J. Wu, U.V. Desai, D. Gao, J. Am. Chem. Soc. 133 (2011) 8122–8125.
[12] A. Mclaren, T. Valdes-Solis, G. Li, S.C. Tsang, J. Am. Chem. Soc. 131 (2009) 12540–12541.
[13] J. Wang, X.M. Fan, K. Tian, Z.W. Zhou, Y. Wang, Appl. Surf. Sci. 257 (2011) 7763–7770.
[14] J. Su, C. Wang, C. Tang, Q. Niu, Y. Zhang, Z. Fu, J. Alloys Compd. 509 (2011) 6102–6105.
[15] K. Jacobs, D. Schulz, D. Klimm, S. Ganschow, Solid State Sci. 12 (2010) 307–310.
[16] Y. Sun, J.H. Seo, C.J. Takacs, J. Seifter, A.J. Heeger, Adv. Mater. 23 (2011) 1679–1683.
[17] K. Govender, D.S. Boyle, P.B. Kenway, P. O'Brien, J. Mater. Chem. 14 (2004) 2575–2591.
[18] M. Kokotov, G. Hodes, J. Mater. Chem. 19 (2009) 3847–3854.
[19] J. Zeng, Y. Zheng, M. Rycenga, J. Tao, Z.-Y. Li, Q. Zhang, Y. Zhu, Y. Xia, J. Am. Chem. Soc. 132 (2010) 8552–8553.
[20] T. Yu, D.Y. Kim, H. Zhang, Y. Xia, Angew. Chem. Int. Ed. 50 (2011) 2773–2777.
[21] D.Y. Kim, W. Li, Y. Ma, T. Yu, Z.-Y. Li, O.O. Park, Y. Xia, Chem. Eur. J. 17 (2011) 4759–4764.
[22] M. Jin, H. Liu, H. Zhang, Z. Xie, J. Liu, Y. Xia, Nano Res. 4 (2011) 83–91.
[23] H. Zhang, W. Li, M. Jin, J. Zeng, T. Yu, D. Yang, Y. Xia, Nano Lett. 11 (2011) 898–903.
[24] X. Xie, Y. Li, Z.-Q. Liu, M. Haruta, W. Shen, Nature 458 (2009) 746–749.
[25] H.G. Yang, C.H. Sun, S.Z. Qiao, J. Zou, G. Liu, S.C. Smith, H.M. Cheng, G.Q. Lu, Nature 453 (2008) 638–642.
[26] H.G. Yang, G. Liu, S.Z. Qiao, C.H. Sun, Y.G. Jin, S.C. Smith, J. Zou, H.M. Cheng, G.Q.M. Lu, J. Am. Chem. Soc. 131 (2009) 4078–4083.
[27] J.-H. Sun, S.-Y. Dong, Y.-K. Wang, S.-P. Sun, J. Hazard. Mater. 172 (2009) 1520–1526.
[28] Y.H. Jang, S.T. Kochuveedu, M.-A. Cha, Y.J. Jang, J.Y. Lee, J. Lee, u. Lee, J. Kim, D.Y. Ryu, D.H. Kim, J. Colloid Interface Sci. 345 (2010) 125–130.
[29] M. Bizarro, A. Sánchez-Arzate, I. Garduno-Wilches, J.C. Alonso, A. Ortiz, Catal. Today 166 (2011) 129–134.
[30] Y.-K. Kim, D.-H. Min, Langmuir 25 (2009) 11302–11306.
[31] W.-J. Li, E.-W. Shi, W.-Z. Zhong, Z.-W. Yin, J. Crystal Growth 203 (1999) 186–196.
[32] R.B. Peterson, C.L. Fields, B.A. Gregg, Langmuir 20 (2004) 5114–5118.
[33] R.L. Penn, J.F. Banfield, Science 281 (1998) 969–971.
[34] Y.-H. Tseng, H.-Y. Lin, M.-H. Liu, Y.-F. Chen, C.-Y. Mou, J. Phys. Chem. C 113 (2009) 18053–18061.
[35] L.P. Bauermann, A.d. Campo, J. Bill, F. Aldinger, Chem. Mater. 18 (2006) 2016–2020.
[36] F. Li, Y. Ding, P. Gao, X. Xin, Z.L. Wang, Angew. Chem. 116 (2004) 5350–5354.
[37] G. Bruno, M.M. Giangregorio, G. Malandrino, P. Capezzuto, I.L. Fragala, M. Losurdo, Adv. Mater. 21 (2009) 1700–1706.
[38] Z. Liu, X.D. Wen, X.L. Wu, Y.J. Gao, H.T. Chen, J. Zhu, P.K. Chu, J. Am. Chem. Soc. 131 (2009) 9405–9412.
[39] L. Jia, W. Cai, H. Wang, H. Zeng, Cryst. Growth Des. 8 (2008) 4367–4371.
[40] A. Taubert, D. Palms, O. Weiss, M.-T. Piccini, D.N. Batchelder, Chem. Mater. 14 (2002) 2594–2601.
[41] J. Zhang, H. Liu, Z. Wang, N. Ming, Z. Li, A.S. Biris, Adv. Funct. Mater. 17 (2007) 3897–3905.
[42] K.X. Yao, H.C. Zeng, J. Phys. Chem. C 111 (2007) 13301–13308.
[43] K.S. Krishna, U. Mansoori, N.R. Selvi, M. Eswaramoorthy, Angew. Chem. 119 (2007) 6066–6069.
[44] R.F. Zhuo, H.T. Feng, J.T. Chen, D. Yan, J.J. Feng, H.J. Li, B.S. Geng, S. Cheng, X.Y. Xu, P.X. Yan, J. Phys. Chem. C 112 (2008) 11767–11775.
[45] Ü. Özgür, Y.I. Alivov, C. Liu, A. Teke, M.A. Reshchikov, S. Doğan, V. Avrutin, S.-J. Cho, H. Morkoçd, J. Appl. Phys. 98 (2005) 041301.
[46] Y.G. Wang, S.P. Lau, H.W. Lee, S.F. Yu, B.K. Tay, J. Appl. Phys. 94 (2003) 354–358.
[47] C.-C. Lin, H.-P. Chen, H.-C. Liao, S.-Y. Chena, Appl. Phys. Lett. 86 (2005) 183103.
[48] H.S. Kang, J.S. Kang, J.W. Kim, S.Y. Lee, J. Appl. Phys. 95 (2004) 1246–1250.
[49] Q. Xu, X. Zhu, F. Zhang, L. Yang, W. Jiang, X. Zhou, Vacuum 84 (2010) 1315–1318.
[50] L.J. Wang, G.J. Exarhos, Thin Solid Films 519 (2010) 1495–1500.
[51] C.A. Arguello, D.L. Rousseau, S.P.S. Porto, Phys. Rev. 181 (1969) 1351–1363.
[52] Y. Wang, X. Li, G. Lu, X. Quan, G. Chen, J. Phys. Chem. C 112 (2008) 7332–7336.
[53] D.-F. Zhang, L.-D. Sun, J. Zhang, Z.-G. Yan, C.-H. Yan, Cryst. Growth Des. 8 (2008) 3609–3615.
[54] J. Li, Z. Chen, X. Wang, D.M. Proserpio, J. Alloys Compd. 262–263 (1997) 28–33.
[55] R.V. Kumar, Y. Diamant, A. Gedanken, Chem. Mater. 12 (2000) 2301–2305.
[56] R.V. Kumar, R. Elgamiel, Y. Koltypin, J. Norwig, A. Gedanken, J. Crystal Growth 250 (2003) 409–417.
[57] E.S. Jang, J.-H. Won, S.-J. Hwang, J.-H. Choy, Adv. Mater. 18 (2006) 3309–3312.
[58] G.R. Li, T. Hu, G.L. Pan, T.Y. Yan, X.P. Gao, H.Y. Zhu, J. Phys. Chem. C 112 (2008) 11859–11864.